

Deuteron structure from $(p, 2p)$ and (d, p) breakup data at medium energies

C. F. Perdrisat

The College of William and Mary, Williamsburg, Virginia 23185

V. Punjabi

Norfolk State University, Norfolk, Virginia 23504

(Received 11 May 1990)

The results of a nonrelativistic calculation of the exclusive ${}^2\text{H}(p, 2p)n$ cross section and inclusive ${}^1\text{H}(\vec{d}, p)X$ cross section and tensor analyzing power T_{20} , based on an expansion of the scattering τ matrix up to double scattering, are presented. Five different wave functions, including Reid with soft core, Paris, Bonn, Amsterdam, and Moscow, as well as two NN phase-shift amplitude sets, VPI and Saclay-Geneva, are used. Detailed comparison with the data available indicates that double scattering is indeed important for both reaction channels. For $(p, 2p)$ the complete calculation removes a discrepancy of a factor of 2 to 8 present if comparison is made with the impulse approximation only; the Paris wave function gives the best results. For (\vec{d}, p) the complete calculation results agree fairly well with both cross section and T_{20} data up to $q=200$ MeV/ c . However, neither an enhancement in $d^2\sigma$, nor an abrupt turn toward less negative T_{20} values, both occurring for $q > 250$ MeV/ c , can be explained by the present calculation. Neither the wave functions nor the NN amplitudes used are Lorentz invariant, but the kinematics is treated relativistically. Possible causes for the discrepancy are briefly discussed.

I. INTRODUCTION

There is now a considerable amount of deuteron breakup data, both from the $(p, 2p)$ and the (\vec{d}, p) reactions, for energies ranging from a few hundreds of MeV to several GeV. The question of whether these data can be used to test model wave functions of the deuteron, or even better, determine the deuteron wave function, has not received a definite answer so far. Can, or do, reactions induced by strong interaction reveal the presence of additional degrees of freedom in the deuteron, besides n and p ? The virtual pions from the meson current are probably better seen in electromagnetic interaction. The presence of the Δ — and N^* isobars, which are predicted to contribute an increasingly important part of the deuteron wave function at very short distances, might be observable in breakup data.

Following the observation of an unexpected, wide peak in the 0° proton spectrum for the breakup of 7.2-GeV deuterons on ${}^{12}\text{C}$ by Ableev *et al.*,¹ it was speculated that this could be the signature of the six-quark component of the deuteron, or of Δ excitation. A consecutive study of the same reaction at a deuteron energy of 4.2 GeV on ${}^{12}\text{C}$,² and then at 2.1 and 1.25 GeV on targets of ${}^1\text{H}$, ${}^4\text{He}$, ${}^{12}\text{C}$, Ti, and Sn indicated³ a similar peak at the same proton momentum, for all targets, if a transformation of the proton momentum to the deuteron center of mass was made. The data in Ref. 3 included both cross sections and tensor analyzing powers T_{20} . Approximate target independence was also observed for T_{20} . The T_{20} measurement of Ableev *et al.*⁴ for 7.4-GeV deuterons on ${}^{12}\text{C}$ confirmed this apparent universal character for the breakup data, for both cross section and T_{20} , with the

deuteron frame proton momentum q playing the role of an approximate scaling variable. Both the energy and the target independence of inclusive cross sections and T_{20} suggest that these observables are determined for a significant part by the internal structure of the deuteron. In this paper we analyze the empirical evidence for one target, hydrogen, on the basis of a simple model of the reaction which lends itself to a parameter-free calculation.

In the case of the exclusive channel ${}^2\text{H}(p, 2p)n$, no direct evidence for a peak corresponding to the one seen in inclusive (\vec{d}, p) has ever been discovered. However, severe deviations from the impulse approximation (IA) are well documented in recent work by Punjabi,⁵ Epstein,⁶ as well as older work (for references see Refs. 5 and 6). It is now apparent, as will be discussed in some detail in the present analysis, that these deviations from IA are due, for a large part, to rescattering. One does expect that Δ (or N^*) excitation should also play a role, but the present work indicates that this role in ${}^2\text{H}(p, 2p)n$ is probably small compared to rescattering.

Here we make an attempt to find a consistent explanation for a number of specific features of the exclusive ${}^2\text{H}(p, 2p)n$ cross-section data at large recoil momenta, and the 0° inclusive ${}^1\text{H}(\vec{d}, p)$ cross section and T_{20} data for all kinematics investigated experimentally so far. The comparison of these different pieces of information is made on the basis of a nonrelativistic calculation including one- and two-step nucleon-nucleon (NN) interactions without isobar excitation and without pions in the intermediate or final states, real or virtual. The calculation is based on a generalized form of the multiple-scattering series of Glauber⁷ truncated to double scattering, keeping only the energy-conserving part of the scattering matrix

as developed by Wallace⁸ for ${}^2\text{H}(p,2p)n$. The numerical input basis consists of noncovariant elastic NN amplitudes obtained from a phase-shift analysis of the NN database by the Virginia Polytechnic Institute and State University (VPI) and Saclay-Geneva¹⁰ Collaborations. Five nonrelativistic deuteron wave functions were used. These include Reid soft core¹¹ (RSC) with 6.47% D state, the ones derived from the Paris¹² and Bonn¹³ NN potentials, with 5.77 and 4.38% D state, respectively, and the quark-model-based wave functions of the Amsterdam¹⁴ and Moscow University¹⁵ groups with 5.47 and 6.78% D state, respectively. In spite of the obvious limitations of this approach, it was thought that the results of such a calculation might help establish whether additional degrees of freedom, besides the nucleon ones, might have a visible effect in the deuteron breakup data presently available.

In Sec. II some details of the calculation will be discussed; in particular, we will show how the kinematics at the two interaction vertices of the two-step diagrams was handled. Likewise, a spurious pole occurring for double scattering will be discussed. In Sec. III the cross-section

$$(d^3\sigma/d\Omega_3 d\Omega_4 dT_3)_M = \frac{p_3 p_4^2}{2(2\pi)^5 32 m_d p_1 |E_5 p_4 - p_5 E_4 \cos\theta_{45}|} \sum_{LS} |\langle \mathbf{p}_3 \mathbf{p}_4 \mathbf{p}_5, L | T | 0, M; \mathbf{p}_1, S \rangle_A|^2, \quad (1)$$

where $L = 1-8$ labels the eight orthogonal final three-nucleon spin states and S is the spin of the incoming proton; the subscript A symbolizes antisymmetrization. In the calculation,

$$T_{LMS} = \langle \mathbf{p}_3 \mathbf{p}_4 \mathbf{p}_5, L | T | 0, M; \mathbf{p}_1, S \rangle$$

is the sum of single- and double-scattering terms; it contains the contributions from six independent terms, including the single pp scattering term IA_{pp} , another single-scattering term with np interaction IA_{np} , and the four double-scattering terms illustrated diagrammatically in Fig. 1. The contribution from the terms, including three or more scatterings, are presumed to be cancelled by the principal part of the propagator $G = 1/(E - H_0 + i\epsilon)$; therefore, only the energy-conserving part of G is kept in the multiple-scattering expansion of the τ matrix, which then has the following terms:

$$\begin{aligned} \tau = & \tau_{p'p} + \tau_{p'n} - i\pi\tau_{p'p}\delta(E - H_0)\tau_{p'n} - i\pi\tau_{p'n}\delta(E - H_0)\tau_{p'p} \\ & - i\pi\tau_{pn}\delta(E - H_0)\tau_{p'p} - i\pi\tau_{pn}\delta(E - H_0)\tau_{p'n}, \quad (2) \end{aligned}$$

where p and n are the constituents of the deuteron and the "prime" labels the incident proton. Only terms which include single and double scattering among the

predictions for the exclusive cross-section measurements of Ref. 6 will be compared with the data. In Sec. IV the calculation of the cross section and tensor analyzing power for the inclusive in-flight breakup of tensor polarized deuterons on hydrogen will be described in some detail and the results compared with the data of Ref. 3. A conclusion will be offered in Sec. V.

II. THE CALCULATION

The calculation is based on the earlier work of Wallace;⁸ it has been partially described in several earlier publications (Refs. 3 and 5) with details given in the thesis of Punjabi.¹⁶ Here we will succinctly repeat the most important features, and concentrate on details of kinematics which were not discussed earlier.

Labeling the particles involved in the reaction ${}^2\text{H}(p,2p)n$ with the numerals 2(1,34)5, the exclusive, threefold differential cross section for a deuteron with spin projection M along the quantization direction, expressed in terms of the scattering matrix elements T , is given by

final-state nucleons have been kept in (2). The neglect of the principle part of G is compatible with the Glauber⁷ approach and, because numerous studies¹⁷ have proven the validity of this approximation, it will not be discussed further here. However, an evaluation of the contribution of the principal part may well be necessary in the near future if a full understanding of the successes and limitations of the present calculation is to be obtained.

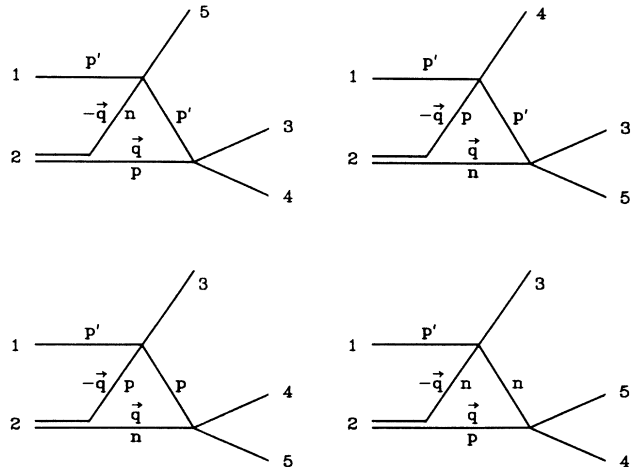


FIG. 1. The four double-scattering diagrams included in the complete calculation, showing the labeling of the reaction participants as used in Sec. II.

For the two IA terms, the T_{LMS} 's take the following form:

$$T_{LMS} = (2\pi)^{3/2} (2m_d)^{1/2} 8\pi\sqrt{s} \times \sum_{m=-1}^{+1} [A_{LMS}(\theta, \phi) \mp A_{LMS}(\pi-\theta, \pi-\phi)] \Phi_M^m(\mathbf{q}), \quad (3)$$

where the A_{LMS} are linear combinations of half-off-shell NN amplitudes as given in Appendix A. These are then approximated by on-shell two-body elastic NN amplitudes $M_{m'm}$, which are the M_{ss} and $M_{l'l}$ ($l', l = -1, 0, 1$) corresponding to transitions between the singlet and triplet states of the interacting NN pair, respectively. As shown in Ref. 5, Sec. II A, the $M_{m'm}$ are evaluated on shell, at an energy and at the pp or pn scattering angles θ and ϕ obtained from the final-state prescription; the energy is given by the invariant energy \sqrt{s} of the interacting NN pair, and the c.m. angles from the invariant four-momentum transfer t , both s and t being calculated in the final state. The \mp sign in Eq. (3) is required for the antisymmetrization of the three-body final state; it is determined by the different symmetry properties of the eight orthogonal final three-nucleon spin states; the sign is $-$ for $L = 1-6$ and $+$ for $L = 7, 8$.

The single-scattering cross section (which is called the impulse approximation IA_{pp} here) then reduces to the well-known form

$$\frac{d^3\sigma}{d\Omega_3 d\Omega_4 dT_3} = \frac{sp_3 p_4^2}{p_1(E_5 p_4 - p_5 E_4 \cos\theta_{45})} \times [M_{1-1}^2 + M_{10}^2 + M_{01}^2 + M_{11}^2 + \frac{1}{2}(M_{ss}^2 + M_{00}^2)] |\Phi(\mathbf{p}_5)|^2 = K (d\sigma/d\Omega)_{c.m.}^{pp} |\Phi(\mathbf{p}_5)|^2, \quad (4)$$

where $|\Phi(\mathbf{p}_5)|^2$ is a theoretical single-nucleon momentum distribution describing the internal motion of the spectator nucleon in the deuteron, here the neutron. K is a phase-space factor and $(d\sigma/d\Omega)_{c.m.}^{pp}$ is the on-shell elastic pp differential cross section in the c.m. frame of the colliding nucleon pair.

For the *first* of the double-scattering diagrams the integration over the component of the internal loop variable \mathbf{q} (see Fig. 1) parallel to $\mathbf{P}_{34} = \mathbf{p}_3 + \mathbf{p}_4$,

$$\int d^2q_{\parallel} \delta(E - E_3 - E_4 - E_5), \quad (5)$$

gives the denominator of the expression for T_{LMS} for the first of the diagrams in Fig. 1:

$$T_{LMS} = \frac{i\pi(2m_d)^{1/2}}{4(2\pi)^{3/2}} \sum_{L'} \sum_{L''} \int_{\mathbf{P}_{34}} d^2q_{\perp} \langle \mathbf{p}_3 \mathbf{p}_4, L | T_{p'p} | \mathbf{P}_{34} - \mathbf{q}, \mathbf{q}, L' \rangle \frac{\langle \mathbf{P}_{34} - \mathbf{q}, \mathbf{p}_5, L' | T_{p'n} | \mathbf{p}_1, \mathbf{q}, L'' \rangle \langle L'' | \Phi(\mathbf{q}) | S \rangle}{|P_{34} E_q - q E_{34} \cos\theta_q|}. \quad (6)$$

For any outside kinematics specified by $(\mathbf{p}_1, \mathbf{p}_3, \mathbf{p}_4, \mathbf{p}_5)$, the denominator in (6) goes through 0, and therefore generates a pole, at a value

$$E_q = \frac{1}{2} E_{34}$$

which corresponds to

$$q = \frac{1}{2} (E_{34}^2 - 4m^2)^{1/2}$$

because, in general,

$$\theta_q^d = \arccos[(-M_{34}^2 \pm 2E_{34} E_q) / 2q P_{34}]. \quad (7)$$

This discontinuity in the integrand of (6) has no physical reality but results from dropping the principal part in G and allowing only one of the particles on the triangle to be off shell. Its effect is limited to a small angular range around θ_q^d and can be eliminated by interrupting the integration accordingly. The error resulting from this approximation is estimated to always remain smaller than 5% in the present calculation.

Similar expressions apply for the three other diagrams of Fig. 1. To calculate the remaining two-fold integral in Eq. (6) over d^2q_{\perp} relative to \mathbf{P}_{34} , we first rewrite it in terms of the singlet-triplet NN amplitudes:

$$T_{LMS} = 2i\sqrt{2m_d} (2\pi)^{3/2} \int_{\mathbf{P}_{34}} d^2q_{\perp} \sum_{m=-1}^{+1} [B_{LMS}^a(\theta, \phi, \theta', \phi') \mp B_{LMS}^a(\pi-\theta, \pi-\phi, \theta', \phi')] \frac{\Phi_M^m(\mathbf{q}) \sqrt{s} \sqrt{s'}}{|P_{34} E_q - q E_{34} \cos\theta_q|}. \quad (8)$$

The B 's are bilinear combinations of the NN amplitudes $M_{m'm}$ which are given in Appendix B.

For fixed kinematics $(\mathbf{p}_1, \mathbf{p}_3, \mathbf{p}_4, \mathbf{p}_5)$ the integration over d^2q_{\perp} can be transformed into one over θ_q , the angle between \mathbf{q} and the total momentum of particles p and p' , which is equal to \mathbf{P}_{34} by momentum conservation. The

momentum q in general is double valued. The relation between q and θ_q is obtained by solving the quadratic kinematical equation for the three-body final state including particles 5, p , and p' (see Fig. 1):

$$q = [P_{34} \epsilon_{34}^2 \cos\theta_q \pm E_{34} (\epsilon_{34}^4 - 4m^2 D^2)^{1/2}] / 2D^2, \quad (9)$$

where

$$D^2 = E_{34}^2 - P_{34}^2 \cos^2 \theta_q, \quad \epsilon_{34}^2 = M_{34}^2 + m_4^2 - m_3^2$$

and

$$M_{34}^2 = E_{34}^2 - P_{34}^2, \quad E_{34} = E_3 + E_4.$$

The limits of the integral are q_- and q_+ obtained with $\cos \theta_q = \pm 1$. The maximum value of θ_q occurs when the argument of the square root in (9) vanishes.

The two-dimensional integral in (8) is carried out numerically by incrementing θ_q from 0 to its maximum value and back to zero, calculating $q(\theta_q)$ at each step, and changing the sign (\pm) in the q solution in (9) as the maximum angle is passed. At each step of θ_q the collision energy and the scattering angles at the first vertex (θ, ϕ), and (θ', ϕ') at the second vertex, are calculated again using the final-state prescription. Then the B 's are calculated from the NN scattering amplitudes at the corresponding angles, and Φ_M^m at the corresponding $q(\theta_q)$ value. The only approximation made in the integration of Eq. (8) is the replacement of the ϕ dependence of the amplitudes by a value averaged over ϕ .

In Ref. 3 we indicated how a relativistically invariant inclusive cross section for ${}^1\text{H}(\vec{d}, pp)$ could be obtained by integrating the threefold cross section, where the detected proton is particle 4 and M is the projection of the deuteron spin:

$$\begin{aligned} \left[\frac{d^3\sigma}{d\Omega_3 d\Omega_4 dp_4} \right]_M &= \frac{1}{2(2\pi)^5} \frac{1}{32m_d} \\ &\times \frac{p_3^2 p_4^2}{p_1 |E_5 p_3 - E_3 p_5 \cos \theta_{35}|} \\ &\times \sum_{LS} |\langle T_{LMS} \rangle_A|^2 \end{aligned} \quad (10)$$

over the full solid angle of unobserved particle 3,

$$\left[\frac{E_4}{p_4^2} \frac{d^2\sigma}{d\Omega_4 dp_4} \right]_M = \frac{E_4}{p_4^2} \int d\Omega_3 \left[\frac{d^3\sigma}{d\Omega_3 d\Omega_4 dp_4} \right]_M. \quad (11)$$

The invariance of Eq. (12) allows one to calculate inclusive (\vec{d}, p) observables with the same code as the exclusive $(p, 2p)$ reaction, provided the calculation is done at $p_1 = p_d/2$ and the angle of particle 4, which is detected at 0° in (\vec{d}, p) , is set to 180° . One feature of this calculation discussed further in Sec. IV A below, is that, as one approaches the kinematic limit in (\vec{d}, p) , which is the maximum laboratory proton momentum occurring when $M_{35} \rightarrow m_n + m_p$, the denominator in the phase-space factor K and the solid angle of particle 3 both tend towards 0, apparently resulting in an increase of the inclusive cross section near the kinematical limit.

III. COMPARISON WITH EXCLUSIVE $(p, 2p)$ DATA

We have calculated the unpolarized exclusive cross sections $d^3\sigma/d\Omega_3 d\Omega_4 dT_3$ for the large recoil momentum data in ${}^2\text{H}(p, 2p)$ at the incident proton energies of 500 MeV in Ref. 6. In this reaction, because of the choice of

kinematics, the dominant interaction is pp and the VPI and Saclay-Geneva phase-shift amplitudes give very similar results; the differences between the results obtained with these two sets of NN amplitudes are of a few percent at most and will not be discussed here. However, the data of Ref. 6 do test the wave function used in the calculation; the Paris, Bonn, and Moscow wave functions give significantly different results in these kinematics with

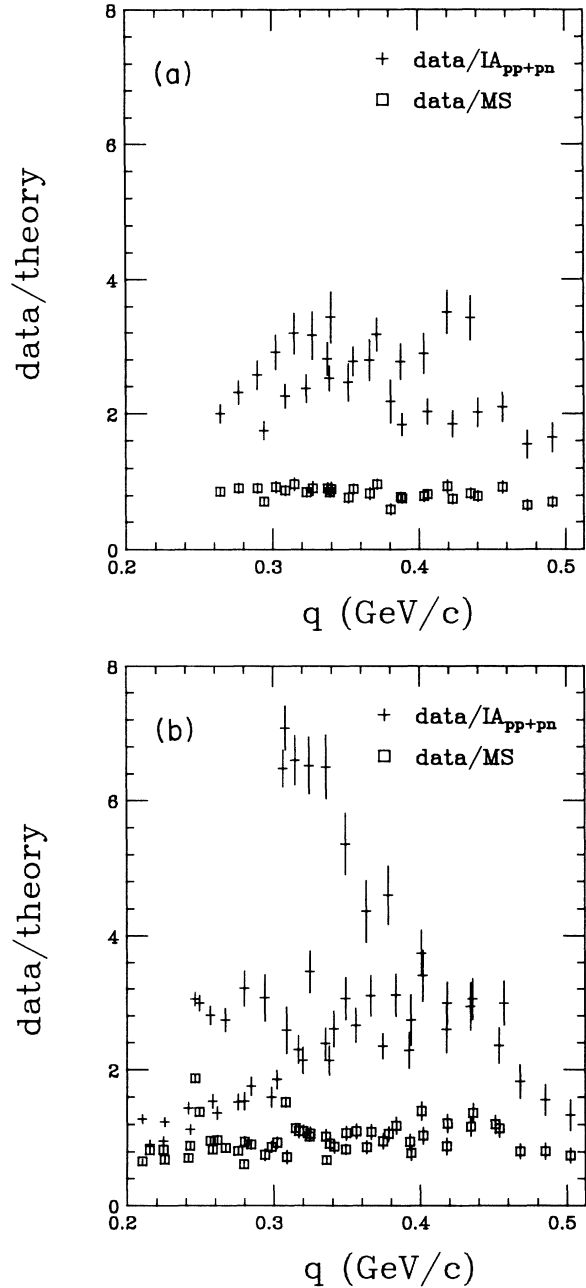


FIG. 2. (a) The ratio (data-theory) for the exclusive ${}^2\text{H}(p, 2p)$ 500-MeV data of Ref. 6. The data are for one proton detected at 14° , the other at 53° , 62° , 73° , and 85° ; the crosses are for the impulse approximation (IA_{pp+pn}), and the squares are for the complete (MS) calculation. The Paris wave function and the VPI NN amplitudes are used. (b) Same as Fig. 1 but for one proton at 30° , the other at 68° , 75° , 83° , and 90° .

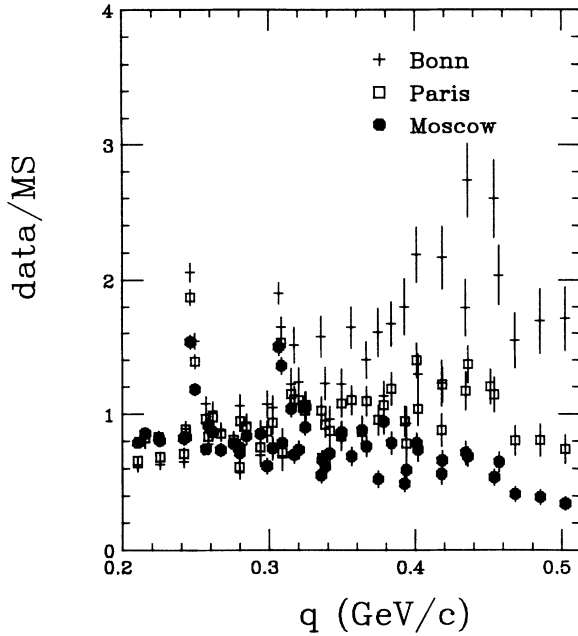


FIG. 3. Same as Fig. 2(b) but for the Moscow wave function (+), the Paris wave function (square), and the Bonn wave function (full circles), in all cases for the complete calculation (*MS*) and VPI *NN* amplitudes. Only the Paris wave functions gives ratios (data-theory) consistently close to 1.

large neutron recoil momenta.

The cross-section data from the same experiment as above, but limited to the small recoil momentum region presented in Ref. 5, were shown to be systematically lower than theory. The discrepancy was about 10% when only the IA *pp* scattering was included, and decreased to approximately 5% when all terms in Eq. (2)

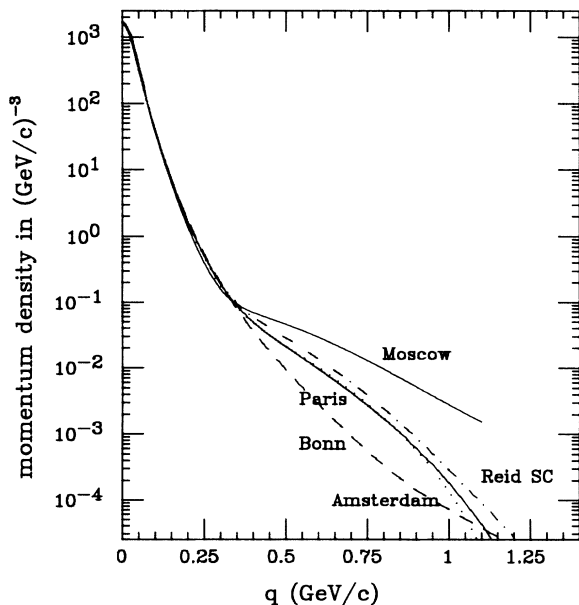


FIG. 4. The momentum-space density for the five wave functions considered: Moscow, Paris, Amsterdam, RSC, and Bonn.

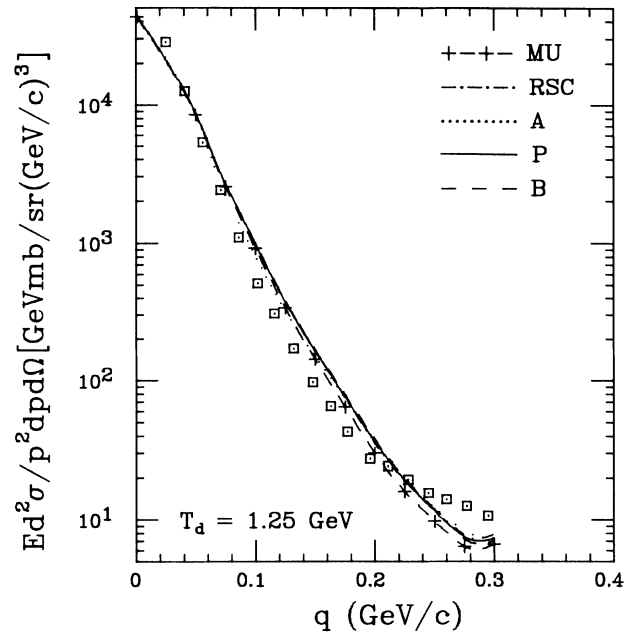


FIG. 5. The inclusive ${}^1\text{H}(d,p)X$ invariant cross section of Ref. 3 at a deuteron energy of 1.25 GeV, plotted versus the proton momentum q in the deuteron frame and compared with the IA ($pp + pn$) for the five wave functions: Paris, Bonn, Amsterdam, Moscow, and RSC. Note the enhancement in the data near the kinematic limit. The *NN* amplitudes are taken from the VPI phase shift.

are included. In the same work, which presented additional data in a number of angle pairs with neutron recoil momenta smaller than 200 MeV/*c*, the full calculation had variable success, usually, but not always, improving the agreement with the data.

Additional data from the same experiment are in Ref.

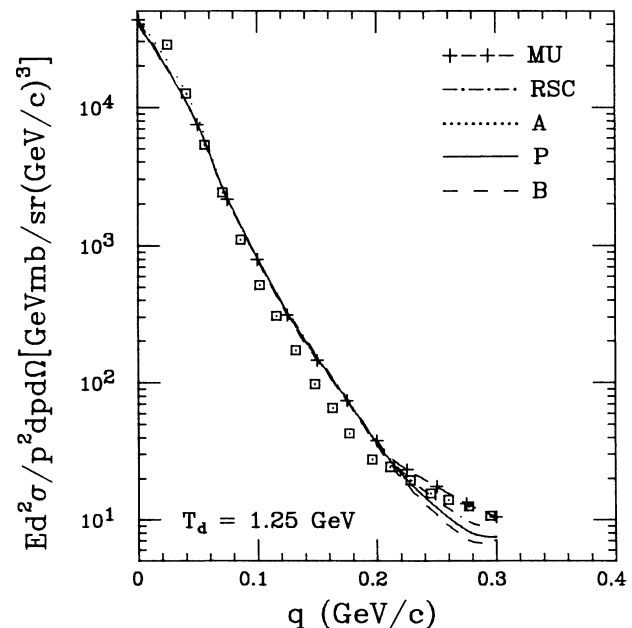


FIG. 6. Same as Fig. 5 but for the complete calculation (*MS*) at 1.25 GeV, with the same five wave functions.

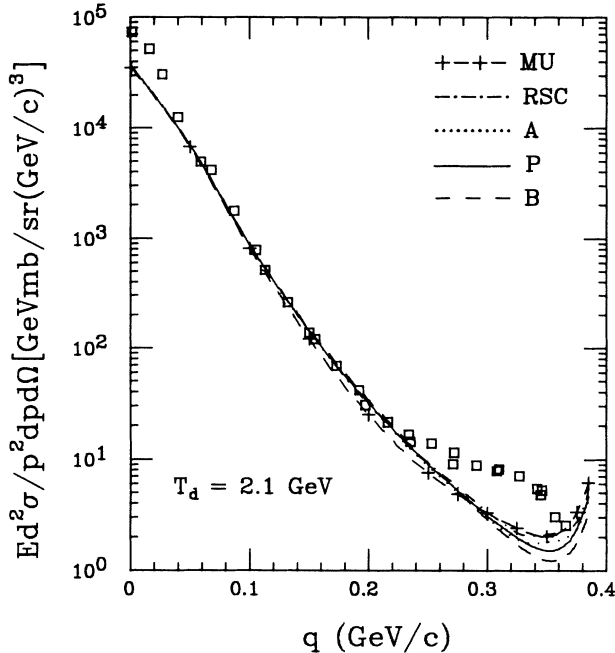


FIG. 7. The inclusive ${}^1\text{H}(d,p)X$ invariant cross section from Ref. 3 at 2.1 GeV compared with the IA ($pn + pp$) for the five wave functions: Paris, Bonn, Amsterdam, Moscow, and RSC. The same enhancement near the kinematic limit is seen as in Fig. 5.

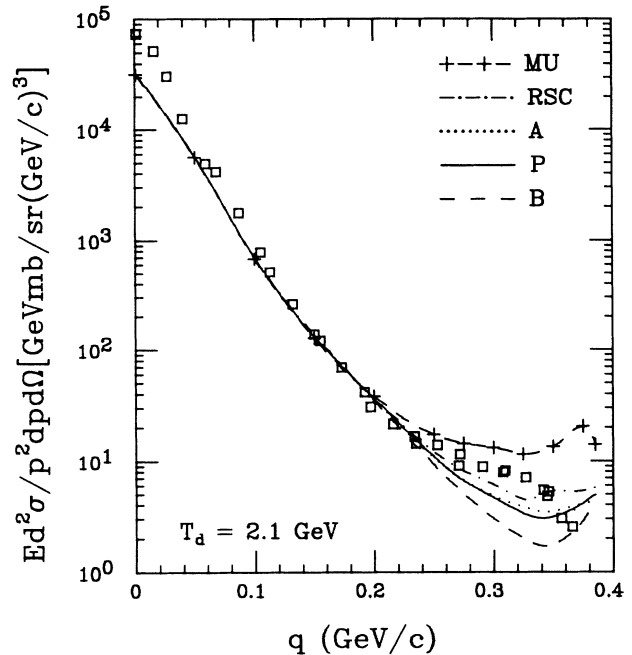


FIG. 8. The same inclusive cross-section data at 2.1 GeV compared with the complete calculation results. The enhancement in the data near $q > 250$ MeV/c is only partially explained with the Paris, Amsterdam, or RSC wave functions. Moscow is too high, Bonn too low.

6, including neutron recoil momenta between 200 and 650 MeV/c. These cross-section data are typically in excess of the IA by factors of 2–8, and as much as 15 at the highest neutron momentum. As shown in Fig. 2 the ratios of the experimental cross sections to the calculated ones become close to 1 when the complete calculation results are used (MS). A ratio close to 1 for (data/theory) would indicate that the calculation reproduces the data. Two families of data with different kinematics are shown here: the first in Fig. 2(a) with one proton detected at 14° and the other proton at 53° , 62° , 73° , and 85° ; the second in Fig. 2(b) with one proton detected at 30° and the other one at 68° , 75° , 83° , and 90° . The deuteron wave function used in the calculation for Fig. 2 is the Paris one and the NV amplitudes are from the VPI phase-shift analysis.

In Fig. 3 the same (data/theory) ratio, again with one proton at 30° as in Fig. 2(b), are shown for the Paris, Bonn, and Moscow wave functions; the agreement is clearly best for the Paris wave function which gives fairly consistently a value of about 0.8 for the ratio (data- MS). The Amsterdam and RSC wave functions give results very close to those for the Paris wave function; these results are not shown to avoid cluttering Fig. 3.

Figure 3 clearly demonstrates that the complete calculation results are strongly wave-function dependent. The reason for this behavior is best understood by looking at Fig. 4 which shows the deuteron single-nucleon momentum densities for the five wave functions used. Up to 350 MeV/c, all five wave functions have densities within $\pm 10\%$ of each other. Moreover, the loop integral for the

double-scattering diagrams requires values of the density from close to $q = 0$ MeV/c up to about 1 GeV/c and in the upper region of q the five wave functions differ notably. Of course, it is not obvious that a single-nucleon wave function makes sense at 1 GeV/c because the NV distances involved are of order 0.2 fm. The smaller double-scattering contribution for the Bonn wave function is clearly related to its relatively small density between 500 MeV/c and 1 GeV/c seen in Fig. 4.

To conclude this part, we have illustrated that, for exclusive ($p, 2p$) data in kinematics far from the quasifree region, the present calculation including the six terms of the multiple-scattering expansion in Eq. (2) is remarkably successful at reproducing the data when the Paris wave function is used. No obvious evidence for virtual Δ excitation is present in the data. Of course, real pions in the final state are excluded by the kinematic constraints of exclusive reactions.

IV. COMPARISON WITH INCLUSIVE (\vec{d}, p) DATA

Comparison of calculation results and data for the inclusive reaction ${}^1\text{H}(\vec{d}, p)X$ of Ref. 3 leads to conclusions which complement the discussion of the exclusive ($p, 2p$) data in Sec. III. The kinematics chosen for the inclusive reaction, with the proton detected at 0° , gives the pn interaction the dominant role for the single-scattering amplitudes, rather than pp as in ($p, 2p$).

In analogy with the notation in Sec. II, the reaction participants in inclusive ${}^1\text{H}(\vec{d}, p)X$ are now labeled with

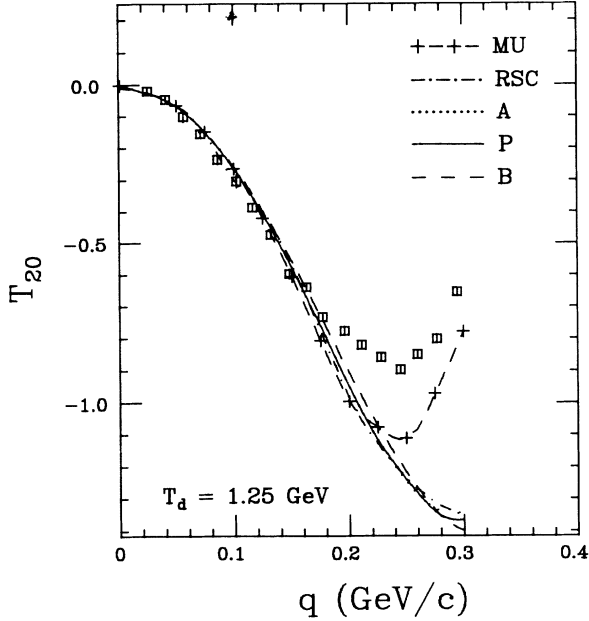


FIG. 9. The T_{20} data of Ref. 3 at 1.25 GeV compared with the IA ($pn + pp$) for the same five functions as above and using the VPI phase-shift NN amplitudes. Only small differences are seen for the various wave functions, with the exception of Moscow.

the numerals 2(1,4)35 for the purpose of the calculation. The data in Ref. 3 are in the form of invariant cross section $E_4 d^2\sigma/p_4^2 dp_4 d\Omega_4$ vs the proton momentum transformed to the projectile deuteron rest frame.

$$q = \gamma_d(p - \beta_d E_p), \quad (12)$$

where p (E_p) is the proton momentum (energy) in the lab-

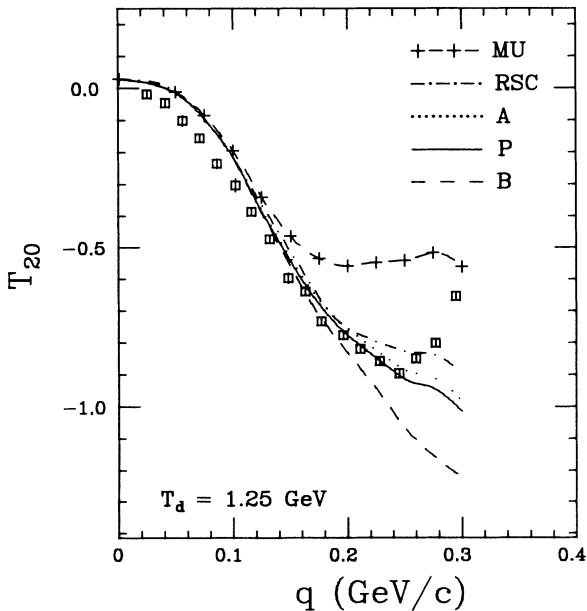


FIG. 10. The T_{20} data of Ref. 3 at 1.25 GeV compared with the complete calculation for the same five wave functions as above. The Paris, Amsterdam, and RSC wave functions give predictions in fair agreement with the data.

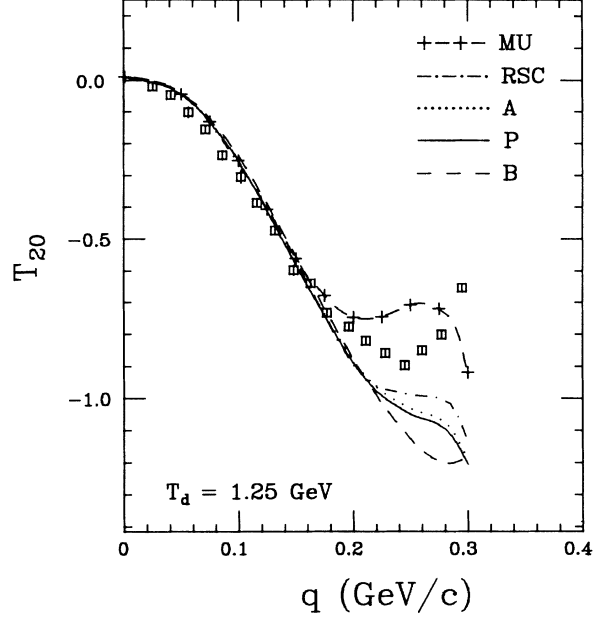


FIG. 11. Same as Fig. 10 but without the contribution of the fourth double-scattering diagram, which includes two consecutive pn interactions. The agreement with the data is worth much, illustrating the importance of this contribution.

oratory frame, and β_d (γ_d) refer to the projectile deuteron. The range of q values extends from $q=0$ when $p_4=p_1/2$, to the kinematic limit corresponding to the missing invariant mass $M_{35}=m_p+m_n$. In the IA with a single pn interaction, q is the momentum of the spectator proton in the deuteron reference frame.

The calculation of inclusive cross sections requires an additional integration compared to the exclusive ones over the phase space of one of the two unobserved final-state nucleons as shown in Sec. II, Eqs. (10) and (11). As a result of the additional integration, both the cross section and the analyzing power T_{20} for a tensor polarized deuteron beam test a much larger region of phase space, and not surprisingly, these observables depend critically upon both the deuteron wave function and the NN amplitudes. At present, the VPI phase-shift amplitudes extend up to 1300 MeV, and the Saclay-Geneva ones are limited to 800 MeV. Because of the energy limitation of the Saclay-Geneva amplitudes, it is possible to compare these two amplitude sets only at the lower deuteron energy ($T_d=1.25$ GeV). Also, it has been pointed out by Arndt¹⁸ that the pn amplitudes are poorly defined by the database above 500 MeV, particularly for polarization observables. The data at 2.1 GeV indicate an extreme sensitivity to the wave function.

A. Inclusive cross sections

The cross-section calculation results for the IA alone, including both pn and pp interactions, are compared to the data at 1.25-GeV deuteron kinetic energy in Fig. 5. It is apparent that the calculation is everywhere within a factor of 2 of the data. There is an indication of an

enhancement in the data near $q > 250$ MeV/c. The sensitivity to the various deuteron wave functions is small. At this deuteron energy pion production is possible only for $q < 180$ MeV/c; above this value of q the missing mass

$$M_x = [(E_1 + m_2 - E_4)^2 - (\mathbf{p}_1 - \mathbf{p}_4)^2]^{1/2} < m_p + m_n + m_\pi .$$

The largest missing mass, at $q = 0$, is

$$M_x = m_p + m_n + (m_\pi + 150 \text{ MeV}) \approx m_N + m_\Delta .$$

The data show no obvious increase of the cross section near the pion threshold. The raise of the total pn cross section is quite gentle compared to the situation in pp scattering, and so it is not surprising that no abrupt effect related to the opening of the inelastic channel is seen in these data.

When the four double-scattering terms are added, we get the curves in Fig. 6, still for 1.25 GeV. The overall agreement with the data is better, even in the region of the enhancement at $q > 250$ MeV/c. The Amsterdam and Paris wave functions give results below the data there. The RSC wave function results are closer, and those with the Moscow wave function, slightly above the data. The Bonn wave function gives the lowest results, as expected from its relatively small D -state probability.

The cross-section data at 2.1-GeV deuteron kinetic energy are compared with the IA ($pn + pp$) prediction in Fig. 7. Here we have better agreement for most q values, but a significant enhancement in the data for $q < 50$ MeV/c and again near the kinematical limit, for $q > 250$ MeV/c. We point out the sharp rise of the theoretical prediction near the kinematic limit. As discussed in Sec. II, the origin of this peak is in the denominator of Eq. (1),

which is exactly zero at the kinematic limit; the data show no indication of it.

Now adding the four double-scattering terms results in the curves shown in Fig. 8. Here the Amsterdam, Paris, and RSC wave functions give approximately the same result for all values of q , including the enhancement region near $q > 250$ MeV/c. The Moscow wave-function prediction is above the data and the results for the Bonn wave functions are below the data, as was the case at the lower deuteron energy. The threshold of π production at 2.1 GeV is near $q = 300$ MeV/c; at $q = 0$ the missing mass

$$M_x = m_p + m_n + (m_\pi + 330 \text{ MeV}) \approx 2m_N + 3m_\pi ,$$

the large experimental cross sections in the region $q < 50$ MeV/c is thus possibly associated with pion production, which is not included in the calculation.

To conclude this part, we find a fair agreement with the data at both deuteron kinematic energies 1.25 and 2.1 GeV for the Amsterdam, Paris, and RSC wave functions. The Moscow wave function tends to overestimate, and the Bonn wave function strongly underestimates the cross section in the region of the enhancement seen in the data at $q > 250$ MeV/c. With the exception of the Moscow wave function with a very large D -state probability, all other wave functions used here underestimate the cross section in the enhancement region. In all cases the differentiation between the five deuteron wave functions investigated comes entirely from the double-scattering terms. As was the case for the exclusive cross section, the strength of the rescattering terms is directly connected to the different momentum densities of these wave functions in the region $q > 300$ MeV/c.

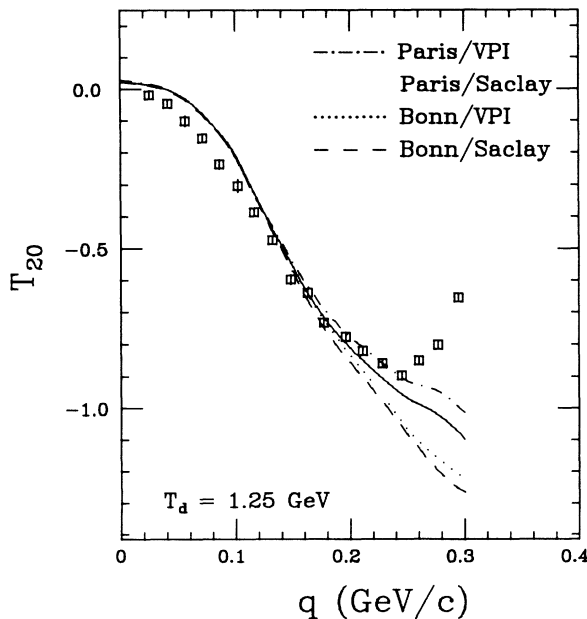


FIG. 12. Same as Fig. 10 but for VPI and Saclay-Geneva phase-shift NN amplitudes, including all four double-scattering diagrams. Significant differences are observed for the Paris wave function.

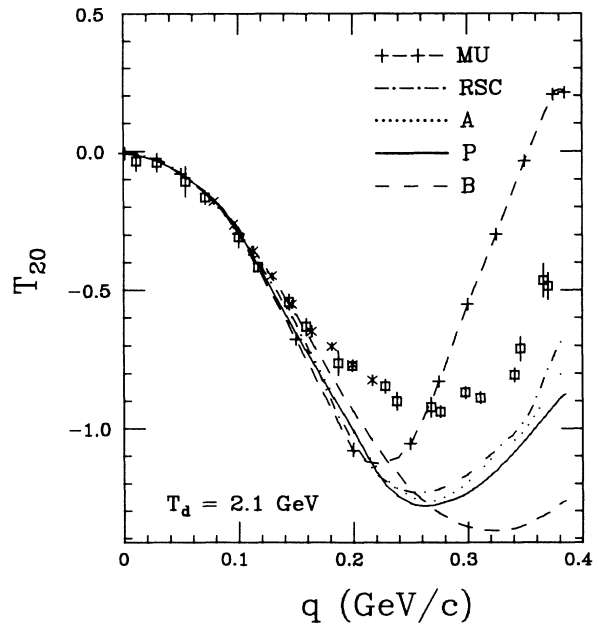


FIG. 13. The T_{20} data of Ref. 3 at a deuteron energy of 2.1 GeV compared with the IA ($pn + pp$) for the same five wave functions; large differences are seen for these wave functions, but none come close to the data.

B. Inclusive tensor asymmetry T_{20}

For polarized spin-1 particles with the quantization axis perpendicular to the beam the (\vec{d},p) cross section at 0° is¹⁹

$$d\sigma = d\sigma_0(1 - \frac{1}{2}\rho_{20}T_{20}) \quad (13)$$

with the $d\sigma_0$ the cross section for unpolarized particles, ρ_{20} the polarization of the incident particle beam and T_{20} the analyzing power of the reaction. Equation (11) in Sec. II gives the cross section for pure M states. To these correspond initial polarizations $\rho_{20} = +\sqrt{2}$ for $M = \pm 1$ and $\rho_{20} = -1/\sqrt{2}$ for $M = 0$. It follows then from (13) that

$$T_{20} = -\sqrt{2} \frac{[d^2\sigma(-1) - 2d^2\sigma(0) + d^2\sigma(+1)]}{[d^2\sigma(-1) + d^2\sigma(0) + d^2\sigma(+1)]}. \quad (14)$$

The T_{20} data of Ref. 3 are shown together with the IA ($pn + pp$) calculation results with VPI NN amplitudes and for 1.25-GeV deuteron kinetic energy in Fig. 9. The agreement between prediction and data up to $q = 200$ MeV/ c is excellent, and the results for the five wave functions differ very little; the VPI NN amplitudes are used here. At larger q values the Moscow wave function gives a distinctly different result, closer to the data than the other four wave functions. Although not displayed, the IA results with Saclay-Geneva NN amplitudes differ little from the ones shown in Fig. 9.

Adding the contribution from the four double-

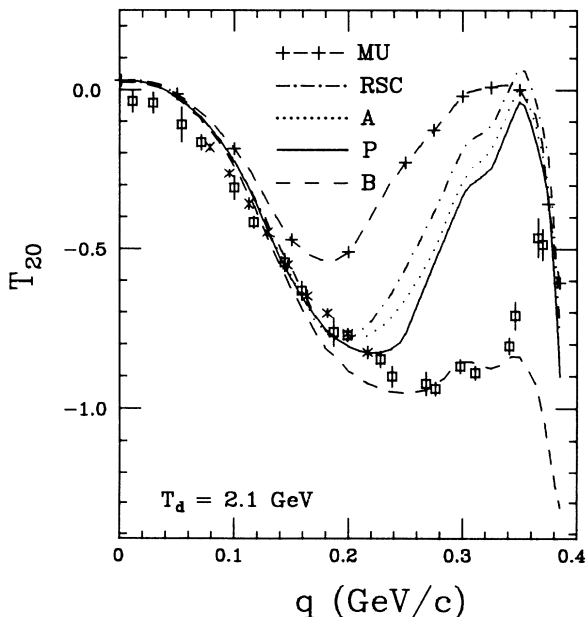


FIG. 14. The same data as in Fig. 13 compared to the results of the complete calculations. Only the Bonn wave function leads to results close to the data.

scattering terms and again with VPI NN amplitudes gives the predictions in Fig. 10. A strong correction to T_{20} is generated by the double-scattering diagrams for each one of the five wave functions. Also, each one of the five wave functions gives distinctly different results, starting already at $q = 150$ MeV/ c . The sensitivity to the wave function is much greater than was the case for the inclusive cross section described in the previous section. Best agreement with the data at $q > 100$ MeV/ c is obtained with the Paris, Amsterdam, and RSC wave functions. But for $q < 100$ MeV/ c , and for all wave functions, the calculation gives T_{20} values which are systematically less negative than the IA in Fig. 9; the agreement with the data is not as good. The results for the Bonn wave functions directly reflect the small D -state probability for this wave function.

As demonstrated in Ref. 18, the pn spin-flip amplitudes are poorly defined by the present data base. These pn amplitudes are more important than the pp amplitudes for (\vec{d},p) at 0° . Therefore, one must expect some uncertainty in the calculation. In particular, the last double-scattering diagram shown in Fig. 1 includes two pn interactions, and it also contributes the largest correction to the IA terms in the region $q > 200$ MeV/ c . Given the uncertainty on pn amplitudes, we show in Fig. 11 the T_{20} values obtained when this diagram is left out. The agreement with the data becomes worse for all of the five wave functions when the contribution of this diagram is removed. We conclude that this is indeed an important double-scattering term for T_{20} , but at the same time its calculation is uncertain. Removing this diagram has a negligible effect on the inclusive cross section in Fig. 6.

A comparison of the results for VPI and Saclay-

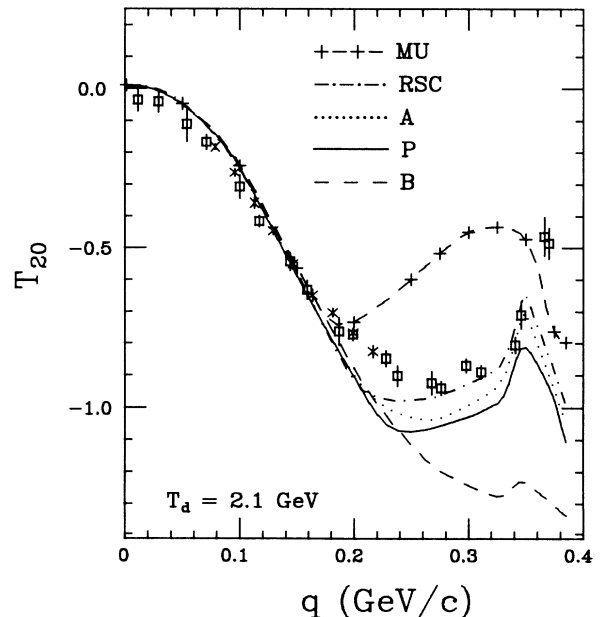


FIG. 15. The same as in Fig. 14 but with the fourth double-scattering diagram removed. Here the Paris, Amsterdam, and RSC wave functions come closer to the data all the way to $q = 350$ MeV/ c .

Geneva NN amplitudes is shown in Fig. 12 for the Paris and Bonn wave functions including all four double-scattering diagrams. A similar sensitivity to the NN amplitudes is observed for the three other wave functions. The calculation using the Paris wave function is more sensitive to the NN amplitudes than the one based on the Bonn wave function; this is directly related to the larger contribution of the double-scattering diagram for the Paris wave function. In general, changing the NN amplitudes produces a smaller change in T_{20} than changing the wave function. Yet we do not feel we can conclude that the calculation is more sensitive to the wave function than to the NN input because the two effects just cannot be isolated.

The T_{20} data of Ref. 3 and the IA ($pn + pp$) calculation results for 2.1-GeV deuteron energy and VPI NN amplitudes are shown in Fig. 13. The five wave functions start to give definitely distinct predictions at $q > 200$ MeV/ c . The results with the Amsterdam, Paris, and RSC wave functions are very close together, but none of the wave functions gives a satisfactory account of the data.

As can be seen in Fig. 14, adding the four double-scattering terms has drastic consequences at this higher deuteron energy, but again it tends to worsen the agreement with the data at small q values. The results with Amsterdam, Paris, RSC, and Moscow wave functions show a drastic turn toward less negative T_{20} values nearer $q = 150\text{--}200$ MeV/ c . The data show a similar turn around but at much larger q (350 MeV/ c). Here, only the Bonn wave function gives results in fair agreement with the data over a large region of q . At 2.1-GeV deuteron energy, only the VPI solution is available presently for the NN amplitudes. Again, because the last double-scattering diagram in Fig. 1 contains two pn interactions for which the amplitudes are uncertain, and also because this diagram affects the calculated T_{20} values most strongly, we show in Fig. 15 the calculation results without the contribution of this diagram. Both the Amsterdam and the RSC wave functions give rather good agreement with the data, but the Paris wave function result is not as good. The Moscow and Bonn wave functions are far off. Again, removing this diagram has only a negligible effect on the cross section in Fig. 8. This point illustrates the fact demonstrated by our calculation that the T_{20} data at 2.1 GeV are indeed very sensitive to the NN amplitudes. A full and consistent understanding of the (\vec{d}, p) reaction will have to await better amplitudes, particularly for pn ; the Saclay-Geneva²⁰ Collaboration is preparing a new set of amplitudes to higher energies than presently available, which will help resolve the apparent inconsistencies revealed in the present analysis.

To conclude, a comparison of the complete T_{20} calculation results at 1.25 and 2.1 GeV in Figs. 10 and 14, respectively, shows that, in both cases, the sharp turn of the experimental T_{20} values toward less negative values near the kinematical limit cannot be explained with any of the wave functions used here. The origin of this effect may be the same than for the inclusive cross-section enhancement in the same region of q at both energies. In both cases the anomalies occur in a region of missing mass just below the π -production threshold.

V. CONCLUSION

To conclude this study, a comparison of the calculation results with the exclusive $(p, 2p)$ cross sections at large recoil momenta indicates that, within the limitations of the model underlying the present calculation, these data are well reproduced when the Paris deuteron wave function is used; similar agreement is obtained with the Amsterdam and RSC wave functions. No sensitivity to the NN amplitudes is found within the accuracy of the data.

The inclusive T_{20} data are partially reproduced with the Paris, Amsterdam, and RSC wave functions, but only when all six diagrams, up to double scattering, are included. The present analysis of the T_{20} data clearly favors a wave function with a D -state probability in the range 5.5–6.5%. The Moscow wave function fails mostly because it contains too many momentum components above 300 MeV/ c . We also have pointed out that the last double-scattering diagram, which involves two consecutive pn interactions, has a very large influence on T_{20} at both energies. Removing it, which might be justified given the uncertainty on the pn amplitudes, results in much worse agreement with the data for all wave functions at 1.25 GeV. However, removing it tends to favor the Bonn wave function at 2.1 GeV. Furthermore, the inclusive (d, p) cross sections are well reproduced by the Paris, Amsterdam, and RSC wave functions, and not significantly affected by the double- pn -scattering term, with the exception of the enhancement at $q > 250$ MeV/ c or by the NN amplitude choice.

In addition, as pointed out in Secs. III and IV, neither the anomaly observed in the inclusive cross section above $q > 250$ MeV/ c , nor the exclusive cross section at large q are well explained with the Bonn wave function when all six diagrams are kept. The Bonn wave function appears to lack the necessary high-momentum components. There is thus a consistent pattern which suggests that both the cross-section enhancement and the abrupt turn of T_{20} towards less negative values, all occurring near $q > 250$ MeV/ c , have a single origin which the deuteron wave functions used here are unable of reproducing. A possible explanation of this observation might be that we are seeing the effect of virtual Δ excitation; it is also possible that the effect is due to either the $\Delta\Delta$ or the six-quark content of the deuteron. But conclusions about these interesting effects must await estimation of the relativistic effects. Nevertheless, it appears unlikely that the universal cross-section enhancement observed in Refs. 1–3 for breakup at several energies and on several targets, all in the vicinity of $q > 250$ MeV/ c , can be explained in terms of rescattering effects only, any more than found in the present work for hydrogen.

The present discussion of the ${}^2\text{H}(p, 2p)n$ and ${}^1\text{H}(d, p)X$ reaction inevitably leads to the conclusion that the most important change necessary is better NN phase-shift amplitudes above 500 MeV. In addition, some of the approximations made in the present calculation, and the neglect of relativistic effects, require further investigation. Evidently new and independent deuteron breakup data could help. A measurement of the spin transfer coefficient in ${}^1\text{H}(\vec{d}, p)$, that is of the proton polarization

for incident vector polarized deuterons, would provide such independent data. Measurements of the polarization transfer both in the exclusive and in the inclusive deuteron breakup channel on hydrogen, are currently underway at the Saturne National Laboratory in Saclay.

ACKNOWLEDGMENTS

This was supported in part by grants from the National Science Foundation (PHY85-09880 and 88-11792) and from the Department of Energy (DE-FG05-8940525).

APPENDIX A

The relation between the on-energy-shell NN matrices and the nonrelativistic center-of-mass scattering amplitude $F_{c.m.}$ is

$$\langle \mathbf{p}_{f_1}, \mathbf{p}_{f_2}, m' | T_{NN} | \mathbf{p}_{i_1}, \mathbf{p}_{i_2}, m \rangle = 8\pi\sqrt{s} \langle m' | F_{c.m.}^{NN}(\theta, \phi) | m \rangle,$$

where $s = (p_{i_1} + p_{i_2})^2 = (p_{f_1} + p_{f_2})^2$ is the invariant-energy squared, θ is the c.m. scattering angle, and ϕ the angle between initial and final reaction planes.

In the equation above $|m\rangle$ is the spin-wave function for a system of two spin- $\frac{1}{2}$ particles. Taking α and β to denote the spin-up and spin-down states, the triplet spin states are

$$\begin{aligned} | +1 \rangle &= \alpha_3 \alpha_4, \\ | 0 \rangle &+ (1/\sqrt{2})(\alpha_3 \beta_4 + \beta_3 \alpha_4), \end{aligned}$$

and

$$| -1 \rangle = \beta_3 \beta_4.$$

Using $m = s$ to denote the singlet state, $|s\rangle = (1/\sqrt{2})(\alpha_3 \beta_4 - \beta_3 \alpha_4)$.

The $\langle m' | F | m \rangle$ are the singlet-triplet representation matrix elements $M_{ss}, M_{11}, M_{1-1}, M_{01}, M_{0-1}, M_{00}, M_{10}, M_{-10}, M_{-11}$, and M_{-1-1} of Stapp *et al.* (Ref. 21). Because of the symmetry properties of the M 's,

$$\begin{aligned} M_{11}(\theta, \phi) &= M_{-1-1}(\theta, -\phi), \quad M_{01}(\theta, \phi) = -M_{0-1}(\theta, -\phi), \\ M_{-11}(\theta, \phi) &= M_{1-1}(\theta, -\phi), \quad M_{10}(\theta, \phi) = -M_{-10}(\theta, -\phi), \end{aligned}$$

there are only six independent M 's.

The representation used for the three-particle spin-wave function $|L\rangle$ is as follows:

$$\begin{aligned} | 1 \rangle &= \alpha_3 \alpha_4 \alpha_5, \\ | 2 \rangle &= \beta_3 \beta_4 \beta_5, \\ | 3 \rangle &= (\beta_3 \alpha_4 \alpha_5 + \alpha_3 \beta_4 \alpha_5 + \alpha_3 \alpha_4 \beta_5) / \sqrt{3}, \\ | 4 \rangle &= (\alpha_3 \beta_4 \beta_5 + \beta_3 \alpha_4 \beta_5 + \beta_3 \beta_4 \alpha_5) / \sqrt{3}, \\ | 5 \rangle &= (\beta_3 \alpha_4 \alpha_5 + \alpha_3 \beta_4 \alpha_5 - 2\alpha_3 \alpha_4 \beta_5) / \sqrt{6}, \\ | 6 \rangle &= (\alpha_3 \beta_4 \beta_5 + \beta_3 \alpha_4 \beta_5 - 2\beta_3 \beta_4 \alpha_5) / \sqrt{6}, \\ | 7 \rangle &= [(\alpha_3 \beta_4 - \beta_3 \alpha_4) \alpha_5] / \sqrt{2}, \\ | 8 \rangle &= [(\beta_3 \alpha_4 - \alpha_3 \beta_4) \beta_5] / \sqrt{2}. \end{aligned}$$

The six initial states of the system are

$$| \mathbf{0}, \mathbf{M}; \mathbf{p}_1, S \rangle = \sum_{L=1}^8 | \mathbf{p}_1, L \rangle \sum_{m=-1}^1 \langle L | \Phi_M^m(\mathbf{q}) | mS \rangle$$

with $M = -1, 0$, and $+1$,

which takes the following forms: first for $S = \alpha$,

$$\begin{aligned} | \mathbf{0}, \mathbf{M}; \mathbf{p}_1, S \rangle &= | \mathbf{p}_1, 1 \rangle \Phi_M^+(\mathbf{q}) + [(\frac{2}{3})^{1/2} | \mathbf{p}_1, 3 \rangle - (\frac{1}{12})^{1/2} | \mathbf{p}_1, 5 \rangle + (\frac{1}{2}) | \mathbf{p}_1, 7 \rangle] \Phi_M^0(\mathbf{q}) \\ &+ [(\frac{1}{3})^{1/2} | \mathbf{p}_1, 4 \rangle + (\frac{1}{6})^{1/2} | \mathbf{p}_1, 6 \rangle - (\frac{1}{2})^{1/2} | \mathbf{p}_1, 8 \rangle] \Phi_M^{-1}(\mathbf{q}), \end{aligned}$$

and for $S = \beta$,

$$\begin{aligned} | \mathbf{0}, \mathbf{M}; \mathbf{p}_1, S \rangle &= | \mathbf{p}_1, 2 \rangle \Phi_M^{-1}(\mathbf{q}) + [(\frac{2}{3})^{1/2} | \mathbf{p}_1, 4 \rangle - (\frac{1}{12})^{1/2} | \mathbf{p}_1, 6 \rangle + (\frac{1}{2}) | \mathbf{p}_1, 8 \rangle] \Phi_M^0(\mathbf{q}) \\ &+ [(\frac{1}{3})^{1/2} | \mathbf{p}_1, 3 \rangle + (\frac{1}{6})^{1/2} | \mathbf{p}_1, 5 \rangle - (\frac{1}{2})^{1/2} | \mathbf{p}_1, 7 \rangle] \Phi_M^+(\mathbf{q}). \end{aligned}$$

Using all the information above the A 's in Eq. (3) for the IA are then calculated using the formula given below. For $S = \alpha$,

$$\begin{aligned} A_{L1\alpha} &= \langle L | F^{pN}(\theta, \Phi) | 1 \rangle, \\ A_{L0\alpha} &= (\frac{2}{3})^{1/2} \langle L | F^{pN}(\theta, \phi) | 3 \rangle - (\frac{1}{12})^{1/2} \langle L | F^{pN}(\theta, \phi) | 5 \rangle + (\frac{1}{2}) \langle L | F^{pN}(\theta, \phi) | 7 \rangle, \\ A_{L-1\alpha} &= (\frac{1}{3})^{1/2} \langle L | F^{pN}(\theta, \phi) | 4 \rangle + (\frac{1}{6})^{1/2} \langle L | F^{pN}(\theta, \phi) | 6 \rangle - (\frac{1}{2})^{1/2} \langle L | F^{pN}(\theta, \phi) | 8 \rangle, \end{aligned}$$

and for $S = \beta$,

$$\begin{aligned} A_{L-1\beta} &= \langle L | F^{pN}(\theta, \phi) | 2 \rangle, \\ A_{L0\beta} &= (\frac{2}{3})^{1/2} \langle L | F^{pN}(\theta, \phi) | 4 \rangle - (\frac{1}{12})^{1/2} \langle L | F^{pN}(\theta, \phi) | 6 \rangle + (\frac{1}{2}) \langle L | F^{pN}(\theta, \phi) | 8 \rangle, \\ A_{L1\beta} &= (\frac{1}{3})^{1/2} \langle L | F^{pN}(\theta, \phi) | 3 \rangle + (\frac{1}{6})^{1/2} \langle L | F^{pN}(\theta, \phi) | 5 \rangle - (\frac{1}{2})^{1/2} \langle L | F^{pN}(\theta, \phi) | 7 \rangle, \end{aligned}$$

where $N = p$ or n .

APPENDIX B

The B 's in Eq. (8) for the first double-scattering terms in Eq. (2) are calculated using the formula given below. For $S = \alpha$,

$$\begin{aligned}
 B_{L1\alpha}(\theta, \phi, \theta', \phi') &= \sum_{L'} \langle L | F^{p'p}(\theta, \phi) | L' \rangle \langle L' | F^{p'n}(\theta', \phi') | 1 \rangle_{\text{sp}}, \\
 B_{L0\alpha}(\theta, \phi, \theta', \phi') &= \sum_{L'} [(\frac{2}{3})^{1/2} \langle L | F^{p'p}(\theta, \phi) | L' \rangle \langle L' | F^{p'n}(\theta', \phi') | 3 \rangle_{\text{sp}} - (\frac{1}{12})^{1/2} \langle L | F^{p'p}(\theta, \phi) | L' \rangle \langle L' | F^{p'n}(\theta', \phi') | 5 \rangle_{\text{sp}} \\
 &\quad + (\frac{1}{2}) \langle L | F^{p'p}(\theta, \phi) | L' \rangle \langle L' | F^{p'n}(\theta', \phi') | 7 \rangle_{\text{sp}}], \\
 B_{L-1\alpha}(\theta, \phi, \theta', \phi') &= \sum_{L'} [(\frac{1}{3})^{1/2} \langle L | F^{p'p}(\theta, \phi) | L' \rangle \langle L' | F^{p'n}(\theta', \phi') | 4 \rangle_{\text{sp}} + (\frac{1}{6})^{1/2} \langle L | F^{p'p}(\theta, \phi) | L' \rangle \langle L' | F^{p'n}(\theta', \phi') | 6 \rangle_{\text{sp}} \\
 &\quad - (\frac{1}{2})^{1/2} \langle L | F^{p'p}(\theta, \phi) | L' \rangle \langle L' | F^{p'n}(\theta', \phi') | 8 \rangle_{\text{sp}}],
 \end{aligned}$$

and for $S = \beta$;

$$\begin{aligned}
 B_{L-1\beta}(\theta, \phi, \theta', \phi') &= \sum_{L'} \langle L | F^{p'p}(\theta, \phi) | L' \rangle \langle L' | F^{p'n}(\theta', \phi') | 2 \rangle_{\text{sp}}, \\
 B_{L0\beta}(\theta, \phi, \theta', \phi') &= \sum_{L'} [(\frac{2}{3})^{1/2} \langle L | F^{p'p}(\theta, \phi) | L' \rangle \langle L' | F^{p'n}(\theta', \phi') | 4 \rangle_{\text{sp}} - (\frac{1}{12})^{1/2} \langle L | F^{p'p}(\theta, \phi) | L' \rangle \langle L' | F^{p'n}(\theta', \phi') | 6 \rangle_{\text{sp}} \\
 &\quad + (\frac{1}{2}) \langle L | F^{p'p}(\theta, \phi) | L' \rangle \langle L' | F^{p'n}(\theta', \phi') | 8 \rangle_{\text{sp}}], \\
 B_{L1\beta}(\theta, \phi, \theta', \phi') &= \sum_{L'} [(\frac{1}{3})^{1/2} \langle L | F^{p'p}(\theta, \phi) | L' \rangle \langle L' | F^{p'n}(\theta', \phi') | 3 \rangle_{\text{sp}} + (\frac{1}{6})^{1/2} \langle L | F^{p'p}(\theta, \phi) | L' \rangle \langle L' | F^{p'n}(\theta', \phi') | 5 \rangle_{\text{sp}} \\
 &\quad - (\frac{1}{2})^{1/2} \langle L | F^{p'p}(\theta, \phi) | L' \rangle \langle L' | F^{p'n}(\theta', \phi') | 7 \rangle_{\text{sp}}].
 \end{aligned}$$

The index (sp) refers to the spectator particles; for this first double-scattering term $\text{sp} = 4$ for the first B in Eq. (8) and $\text{sp} = 3$ for the second B , as required by antisymmetrization. Similar expressions for the B 's hold for the three other double-scattering terms in Eq. (2).

- ¹V. G. Ableev, D. A. Abdushukorov, S. A. Avramenko, Ch. Dimitrov, A. Filipkowski, A. P. Kobushkin, D. K. Nikitin, A. A. Nomofilov, N. M. Piskunov, N. M. Sharov, I. M. Sitnik, E. A. Strokovsky, L. N. Strunov, L. Vizireva, G. G. Vorobiev, and S. A. Zaporozhets, Nucl. Phys. **A393**, 491 (1983).
- ²L. Anderson, W. Bruckner, E. Moeller, S. Nagamiya, S. Nissen-Meyer, L. Schroeder, G. Shapiro, and H. Steiner, Phys. Rev. C **28**, 1224 (1983).
- ³V. Punjabi, C. F. Perdrisat, P. Ulmer, C. Lyndon, J. Yonnet, R. Beurtey, M. Boivin, J. P. Didelez, R. Frascaria, T. Reposeur, R. Siebert, A. Boudard, F. Plouin, and P. C. Gugelot, Phys. Rev. C **39**, 608 (1989).
- ⁴V. G. Ableev, S. V. Dshemuchadze, S. V. Fedukov, V. V. Fimushkin, A. D. Kirillov, A. P. Kobushkin, V. I. Kotov, B. Kuehn, P. K. Manyakov, V. A. Monchinsky, B. Naumann, L. Naumann, W. Neubert, A. A. Nomofilov, S. A. Novikov, L. Penchev, J. K. Pilipenko, N. M. Piskunov, P. A. Rukoyatkin, V. I. Sharov, I. M. Sitnik, E. A. Strokovsky, L. N. Strunov, A. L. Svetov, L. Vizireva, V. I. Volkov, and S. A. Zaporozhets, Pis'ma Zh. Eksp. Teor. Fiz. **47**, 558 (1988) [JETP Lett. **47**, 649 (1988)].
- ⁵V. Punjabi, K. A. Aniol, A. Bracco, C. A. Davis, M. B. Epstein, H. P. Gubler, J. P. Huber, W. P. Lee, D. J. Margaziotis, C. F. Perdrisat, P. R. Poffenberger, H. Postma, H. J. Sebel, A. W. Stetz, and W. T. H. van Oers, Phys. Rev. C **38**, 2728 (1988).
- ⁶M. B. Epstein, J. P. Huber, K. A. Aniol, A. Bracco, C. A. Davis, H. P. Gubler, W. P. Lee, D. J. Margaziotis, C. F. Perdrisat, P. R. Poffenberger, H. Postma, V. Punjabi, H. J. Sebel, A. W. Stetz, and W. T. H. van Oers, Phys. Rev. C **42**, 510 (1990).
- ⁷R. G. Glauber, in *Lectures in Theoretical Physics*, edited by W. E. Brittin and L. G. Dunham (Interscience, New York, 1959), Vol. I, p. 315.
- ⁸J. M. Wallace, Phys. Rev. C **5**, 609 (1972).
- ⁹R. A. Arndt, L. D. Roper, R. A. Bryan, R. B. Clark, B. J. VerWest, and P. Signell, Phys. Rev. D **28**, 97 (1983). Phase shifts from SAID SP88 0-1.3 GeV, and R. A. Arndt, J. S. Hyslop, III, and L. D. Roper, Phys. Rev. D **35**, 128 (1988).
- ¹⁰J. Bystricky, C. Lechanoine-Leluc, and F. Lehar, J. Phys. (Paris) **48**, 199 (1987).
- ¹¹R. V. Reid, Ann. Phys. (N.Y.) **50**, 411 (1968).
- ¹²M. Lacombe, B. Loiseau, R. Vinh Mau, J. Cote, P. Pires, and R. de Tourreil, Phys. Lett. **101B**, 139 (1981).
- ¹³R. Machleidt, Adv. Nucl. Phys. **19**, 189 (1989).
- ¹⁴H. Dijk and B. L. G. Bakker, Nucl. Phys. **A494**, 438 (1989).
- ¹⁵V. M. Krasnopol'sky, V. I. Kukul'in, V. N. Pomerantsev, and P. B. Sazonov, Phys. Lett. **165B**, 7 (1985).
- ¹⁶V. Punjabi, Ph.D. thesis, College of William and Mary, 1986.
- ¹⁷See, for example, D. R. Harrington, Phys. Rev. **184**, 1745 (1969).
- ¹⁸R. A. Arndt, Phys. Rev. D **37**, 2665 (1988).
- ¹⁹J. Arvieux, S. D. Baker, R. Beurtey, M. Boivin, J. M. Cameron, T. Hasegawa, D. Hutcheon, J. Banaigs, J. Berger, A. Codino, J. Duffo, L. Goldzahl, F. Plouin, A. Boudard, G. Gaillard, Nguyen Van Sen, and C. F. Perdrisat, Nucl. Phys. **A431**, 613 (1984).
- ²⁰C. Lechanoine-Leluc (private communication).
- ²¹H. P. Stapp, T. J. Ypsilantis, and N. Metropolis, Phys. Rev. **105**, 302 (1957).